PIBB 生物化学与生物物理进展
Progress in Biochemistry and Biophysics
2025, 52(11): 2842~2853
www.pibb.ac.cn

Catalpol Promotes Differentiation of Neural Stem Cells into Oligodendrocyte *via* Caveolin−1−dependent Pathway in The 3D Microfluidic Chip*

WANG Ya-Chen[1,2], WANG Liang[1,2], SHEN Li-Ming[1,2], LIU Jing[1,2]**

([1])*Stem Cell Clinical Research Center, the First Affiliated Hospital of Dalian Medical University, Dalian* 116000, China;
[2])*Dalian Innovation Institute of Stem Cell and Precision Medicine, Dalian* 116000, China)

Graphical abstract

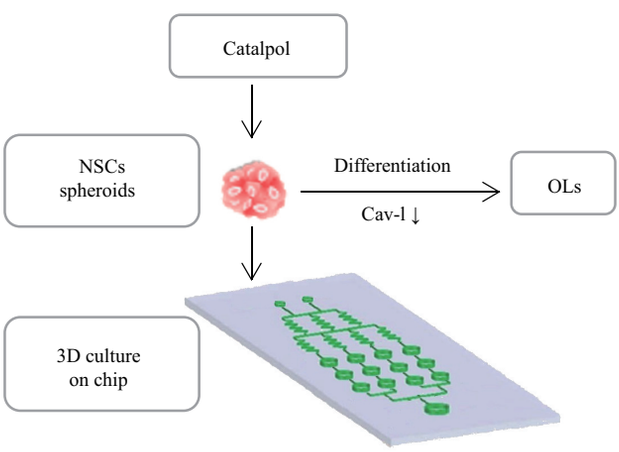

Abstract **Objective** Cerebral palsy (CP) is a prevalent neurodevelopmental disorder acquired during the perinatal period, with periventricular white matter injury (PWMI) serving as its primary pathological hallmark. PWMI is characterized by the loss of oligodendrocytes (OLs) and the disintegration of myelin sheaths, leading to impaired neural connectivity and motor dysfunction. Neural stem cells (NSCs) represent a promising regenerative source for replenishing lost OLs; however, conventional two-dimensional (2D) *in vitro* culture systems lack the three-dimensional (3D) physiological microenvironment. Microfluidic chip technology has emerged as a powerful tool to overcome this limitation by enabling precise spatial and temporal control over 3D microenvironmental conditions, including the establishment of stable concentration gradients of bioactive molecules. Catalpol, an iridoid glycoside derived from traditional medicinal plants, exhibits dual antioxidant and anti-apoptotic properties. Despite its therapeutic potential, the capacity of catalpol to drive NSC differentiation toward OLs under biomimetic 3D conditions, as well as the underlying molecular mechanisms, remains poorly understood. This study aims to develop a microfluidic-based 3D biomimetic platform to systematically investigate the concentration-dependent effects of catalpol on promoting NSCs-to-OLs differentiation and

* This work was supported by grants from the Liaoning Province Excellent Talent Program Project (XLYC1902031) , Dalian Science and Technology Talent Innovation Plan Grant (2022RG18), and Basic Research Project of the Department of Education of Liaoning Province (LJKQZ20222395).
** Corresponding author.
Tel: 86-411-83635963, E-mail: liujing@dmu.edu.cn
Received: July 17, 2025 Accepted: November 3, 2025

to elucidate the role of the caveolin-1 (Cav-1) signaling pathway in this process. **Methods** We developed a novel multiplexed microfluidic device featuring parallel microchannels with integrated gradient generators capable of establishing and maintaining precise linear concentration gradients (0−3 g/L catalpol) across 3D NSCs cultures. This platform facilitated the continuous perfusion culture of NSC-derived 3D spheroids, mimicking the dynamic *in vivo* microenvironment. Real-time cell viability was assessed using Calcein-AM/propidium iodide (PI) dual staining, with fluorescence imaging quantifying live/dead cell ratios. Oligodendrocyte differentiation was evaluated through quantitative reverse transcription polymerase chain reaction (qRT-PCR) for *MBP* and *SOX10* gene expression, complemented by immunofluorescence staining to visualize corresponding protein changes. To dissect the molecular mechanism, the Cav-1-specific pharmacological inhibitor methyl-β-cyclodextrin (MCD) was employed to perturb the pathway, and its effects on differentiation markers were analyzed. **Results** Catalpol demonstrated excellent biocompatibility, with cell viability exceeding 96% across the entire tested concentration range (0−3 g/L), confirming its non-cytotoxic nature. At the optimal concentration of 0−3 g/L, catalpol significantly upregulated both MBP and SOX10 expression (P<0.05, P<0.01), indicating robust promotion of oligodendroglial differentiation. Intriguingly, *Cav-1* mRNA expression was progressively downregulated during NSC differentiation into OLs. Further inhibition of Cav-1 with MCD further enhanced this effect, leading to a statistically significant increase in OL-specific gene expression (P<0.05, P<0.01), suggesting Cav-1 acts as a negative regulator of OLs differentiation. **Conclusion** This study established an integrated microfluidic gradient chip-3D NSC spheroid culture system, which combines the advantages of precise chemical gradient control with physiologically relevant 3D cell culture. The findings demonstrate that 3 g/L catalpol effectively suppresses Cav-1 signaling to drive NSC differentiation into functional OLs. This work not only provides novel insights into the Cav-1-dependent mechanisms of myelination but also delivers a scalable technological platform for future research on remyelination therapies, with potential applications in cerebral palsy and other white matter disorders. The platform's modular design permits adaptation for screening other neurogenic compounds or investigating additional signaling pathways involved in OLs maturation.

Key words catalpol, neural stem cells, oligodendrocytes, differentiation, caveolin-1, microfluidic chip
DOI：10.3724/j.pibb.2025.0337 **CSTR**：32369.14.pibb.20250337

Periventricular white matter injury (PWMI) constitutes the primary neuropathological basis of cerebral palsy (CP), driving lifelong neuromotor disability through arrested oligodendrocyte maturation and disrupted myelination[1-2]. Contemporary evidence confirms that oligodendrocytes (OLs) exhibit selective vulnerability during critical developmental windows, with CP cases demonstrating permanent hypomyelination[3-4]. Despite extensive research, current therapies exhibit limited efficacy in promoting remyelination. While neural stem cells (NSCs) transplantation holds regenerative potential, conventional two-dimensional (2D) *in vitro* systems—despite their operational convenience and high reproducibility—display insufficient translational relevance[5-6].

Researchers therefore balance microenvironmental complexity against system reliability when developing advanced *in vitro* models. Emerging microfluidic platforms enable high-precision modulation of stem cell microenvironments[7]—a technological revolution that synergizes with catalpol, a bioactive iridoid glycoside from Rehmannia glutinosa demonstrating multimodal neuroprotective properties[8]. Hassan *et al.*[9] showed catalpol rescues mitochondrial function in oxidative stress, while Chao *et al.*[8] specifically confirmed its anti-apoptotic action on OLs. Significantly, catalpol's potential to drive NSCs lineage commitment toward oligodendrogenesis remains unexplored. This knowledge gap is significant given NSCs' potential as a therapeutic OL source.

Caveolin-1 (Cav-1) plays critical roles in oligodendrocyte biology. Cai *et al.*[10] established that Cav-1 deficiency enhances oligodendrocyte maturation in *in vivo* models[7]. Leveraging this insight, we employed a microfluidic concentration-gradient system to screen catalpol's effect on NSCs differentiation. At 3 g/L, catalpol significantly enhanced OLs generation concomitant with Cav-1 downregulation. Crucially, Cav-1 overexpression abolished catalpol's prodifferentiation effects, confirming Cav-1 suppression mediates this process. This represents the first integration of catalpol pharmacology with microfluidic technology for targeted oligodendrogenesis.

1 Materials and methods

1.1 Design and fabrication of the microfluidic device

We designed a microfluidic device with a concentration gradient generator (CGG) (Figure 1). The device is composed of a polydimethylsiloxane (PDMS) microfluidic chip covered with a PDMS-coated glass slide. The microfluidic chip, which constitutes the lower layer of the device, was designed with multi-channel connections including fluid inlets, CCG, a 3×4 array of cell culture chambers, and an outlet. The perfusion channels were 300 μm×300 μm (width and height) and the culture chambers were 2.5 mm×2 mm (diameter×height) in size. The upper layer (the PMDS-coated glass cover) was used as the 3D cell culture surface.

Microfluidic chips were fabricated by casting PDMS against a master, which was patterned from SU8-3035 negative photoresist (Microchem, USA) using conventional soft lithography. The PDMS base and curing agent (Dow Corning, USA) were mixed together at a ratio of 10∶1 and poured onto the master, which was then heated at 80℃ for 60 min. After cooling, the PDMS layer was gently peeled off from the master. Holes were punched for inlets, cell culture chambers, and outlets. PDMS was spin-coated and solidified on clear glass slides, which were irreversibly attached to the microfluidic chip using PDMS-PDMS bonding, and cured in an oven at 80℃ for 45 min. The cell culture region of the PDMS slide was aligned to the chamber region of the microfluidic chip. After sealing, only the inlet and outlet ports were open for fluidic access. Prior to the experiments, the device was UV-sterilized for 120 min.

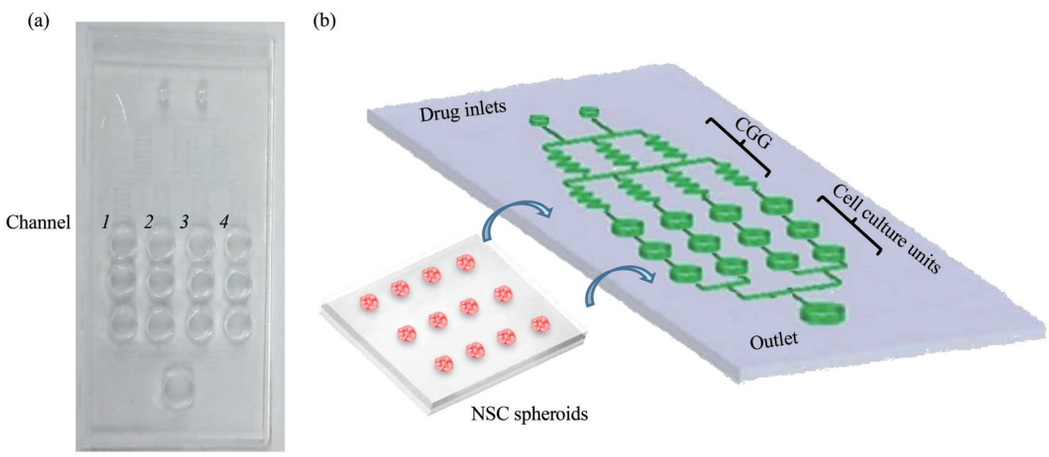

Fig. 1 Overview of the microfluidic array used for testing catalpol sensitivity on NSCs differentiation

(a) Photograph of the established model. (b) Neural culture platform of the microfluidic-based chamber system.

1.2 Isolation and culture of NSCs

Sprague-Dawley (SD) rats were purchased from the Experimental Animal Center of Dalian Medical University. NSCs were freshly isolated from the cortex of a 13-day-old rat embryo, and expanded in a medium supplemented with mitogenic factors, namely epidermal growth factor (EGF) and basic fibroblast growth factor (bFGF). The maintenance of undifferentiated NSCs was confirmed by neurosphere formation and expression of the undifferentiated NSCs markers nestin and Sox2 (Ethical Review No. LL2020012).

1.3 NSCs spheroids and seeding of the microfluidic device

A single cell suspension at a concentration of 1.0×10^6/ml was seeded on a PDMS membrane-covered glass slide, which was upended in a medium-filled culture dish for 2 d to form NSCs spheres. These were then used to seed the medium-filled microfluidic device, which was upended following inoculation. The flow rate was set to 1 μl/min. A medium volume of 1.44 ml was required for each run of 24 h, and was supplied in a single round-robin fashion. Removal of medium containing metabolic

waste was performed through a discharge dish tube.

1.4 Cell viability assay

Cell viability was determined by staining the cells with Calcein-AM/PI (Sigma, USA). The construct was washed twice with PBS for 5 min. Calcein-AM/PI staining was then performed using 1 μmol/L calcein and propidium iodide (PI) in PBS. The sample was incubated with the dyes for 30 min, after which the excess dye solution was removed and the constructs was washed twice with PBS for 5 min. Cell viability was calculated as the ratio between live and total cells, with cell numbers determined by counting the cells in 5 different microscopic fields. Live and dead cells display green and red fluorescence, respectively. The images were analyzed and the cell viability calculated using an IPP 5.0 system.

1.5 Fluorescence staining and imaging

Prior to immunostaining, the sample was removed from the culture medium and washed twice with PBS. The sample was then incubated in 4 % paraformaldehyde solution at 4°C overnight, and then incubated in PBS containing 1% BSA for 1 h at 37℃. After blocking, the sample was incubated at 4℃ overnight with primary antibodies anti-MBP, anti-SOX10 and anti-Cav-1 (Abcam, 1∶500). After 3 rinses with PBS to remove the free primary antibodies, the sample was incubated with secondary antibodies (1∶100), namely anti-Rabbit IgG-FITC and anti-mouse IgG-TRITC (Sigma, USA) at room temperature for 1.5 h, and rinsed with PBS. Subsequently, the sample was dyed with Hoechest as chromogen for 5 min, and then washed twice with PBS and once with pure water. Stained cells were viewed using a confocal laser scanning microscope. The IPP 5.0 system was used to analyze the images.

1.6 Quantitative real−time reverse transcription PCR（qRT−PCR）

NSCs spheroids were collected from the disassembled microfluidic array device and quantified by qRT-PCR. Total RNA was isolated from each sample. cDNA was generated from the purified RNA using a PrimeScript™ RT reagent Kit (Takara, Japan) according to the manufacturer's instructions. qRT-PCR was performed in a Thermal Cycler Dice Real Time System (Takara, Japan) by mixing 2 μl of the synthesized cDNA with SYBR® Premix Ex Taq™ II reagents (Takara, Japan) and appropriate primers according to the manufacturer's protocol. The primer sequences are provided in Table 1.

Table 1 Forward and reverse primer sequences used for RT−PCR (*GAPDH* as a housekeeping gene)

Gene		Primer sequence
GAPDH	Forward	5'-GGCACAGTCAAGGCTGAGAATG-3'
	Reverse	5'-ATGGTGGTGAAGACGCCAGTA-3'
Cav-1	Forward	5'-GCCCTCACAGGGACATCTCTACA-3'
	Reverse	5'-CCGCAATCACATCTTCAAAGTCA-3'
MBP	Forward	5'-ATGGTGAGATTCACCGAGGA-3'
	Reverse	5'-CATTGTTCTGGATCGCATCTG-3'
SOX10	Forward	5'-CGCACCTCCACAATGCTGA-3'
	Reverse	5'-GAGGTTGGTACTTGTAGTCCGGATG-3'

1.7 Statistical analysis

The data was presented as mean±SD. Error bars in the figures depict the standard deviation of at least three biological samples. ANOVA and student *t*-test were performed for statistical comparison.

2 Results

2.1 Microfluidic array for catalpol sensitivity of 3D cultures

We developed a microfluidic device with a CGG and investigated the susceptibility of NSCs to catalpol. Compound susceptibility and NSCs differentiation were assessed simultaneously. As reported previously[11], 4 drug concentrations were generated in channels *1−4* of the device. Catalpol was introduced at 3 g/L into one device inlet, whereas culture medium without test compound was pumped simultaneously into another device inlet. The catalpol concentration in channels *1*, *2*, *3*, and *4* was 0, 1, 2, and 3 g/L, respectively, and the insulin-like growth factor (IGF) concentrations were 0, 500, 1 000, and 1 500 μg/L, respectively. In our study, IGF was used as the positive control compound that promotes NSCs differentiation into OLs[12]. The device design allowed for the input of NSCs spheroids into all 12 units at the same time (Figure 1).

2.2 Cell viability assay

The NSCs were cultured using four catalpol concentrations: 0, 1, 2, and 3 g/L. The viability of the NSCs was determined using direct staining of dead

and live cells as shown in Figure 2a. Moreover, on the basis of the ratio of the number of nuclei stained with Hoechst 33258 to the total number of calcein-stained cells, the viability scores of cells in the test groups were 97.42% for 0 g/L, 97.72% for 1 g/L, 97.48% for 2 g/L, and 96.75% for 3 g/L after 4 d of culture (Figure 2b). The viability scores of cells in the test groups were 96.36% for 0 g/L, 94.16% for 1 g/L, 97.99% for 2 g/L, and 97.25% for 3 g/L after 7 d of culture (Figure 2c). This observation indicated that NSCs retain good cell viability at the tested catalpol concentrations.

The NSCs were cultured at four IGF concentrations as positive control (0, 500, 1 000, 1 500 μg/L). The viability of the NSCs was consistent with that of the catalpol groups (Figure S1).

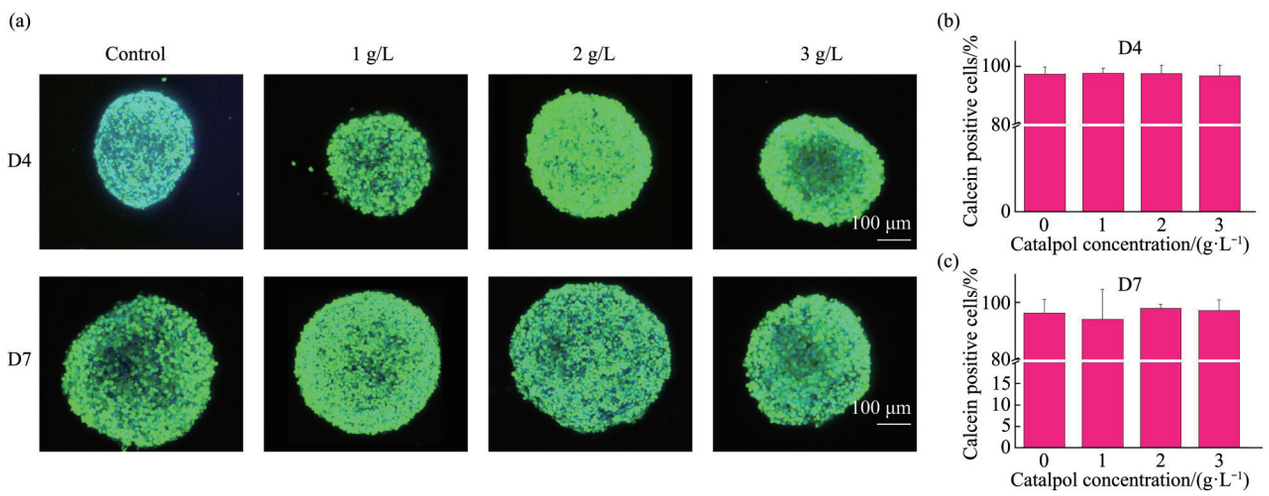

Fig. 2 Viability of NSCs under four catalpol concentrations

(a) Confocal microscopic characterization of NSCs after 4 d and 7 d of incubation. All the images were being overlaid, live cells (green) and dead cells (red). (b, c) Quantitative analysis of live NSCs percentages in each group. The data are shown as mean±SD (n=5). Error bars indicate the SEM relative to the control.

2.3 Catalpol promotes NSCs differentiation

NSCs differentiation in 3D microfluidic culture was quantified by qRT-PCR analysis of the samples following culture of NSCs for 4 and 7 d. The results demonstrated a concentration-dependent upregulation of SOX10, a key transcription factor for OLs, after 4 d of perfusion culture. Specifically, the 1, 2, and 3 g/L catalpol groups showed increases of 86.1%, 42.6%, and 76.2%, respectively, with the 1 and 3 g/L groups exhibiting statistically significant differences (P<0.05) (Figure 3a). By day 7, the expression changes in the respective concentration groups were 11.4%, 42.9%, and 160.0%. The 3 g/L group displayed the most substantial upregulation, which was highly significant (P<0.01) (Figure 3b). Similarly, the expression of the *MBP* gene after 4 d of perfusion culture was upregulated by 45.2%, 17.4%, and 71.3% in the 1, 2, and 3 g/L catalpol groups, respectively, compared to the control group (Figure 3a). The increases in the 1 and 3 g/L groups were statistically significant (P<0.05, P<0.01). By day 7, the expression levels in the concentration groups had further changed, showing increases of 92.8%, 1.6%, and 123.2%. The 1 and 3 g/L groups maintained a significant upregulation (P<0.01) (Figure 3b), indicating that the enhancing effect of catalpol on *MBP* expression is both concentration- and time-dependent. These findings further support that 3 g/L is the optimal concentration for promoting oligodendrocyte differentiation.

As shown in the immunofluorescence images in Figures 3c, d, co-localization analysis was performed for the oligodendrocyte markers SOX10 (green) and MBP (red). This provides a qualitative assessment for the qRT-PCR findings.

To systematically evaluate the promoting effect of IGF on oligodendrocyte differentiation, this study established four IGF concentration groups as positive

controls. Quantitative qPCR analysis results showed that 500−1 000 μg/L IGF significantly upregulated the expression of SOX10 and MBP (Figure S2).

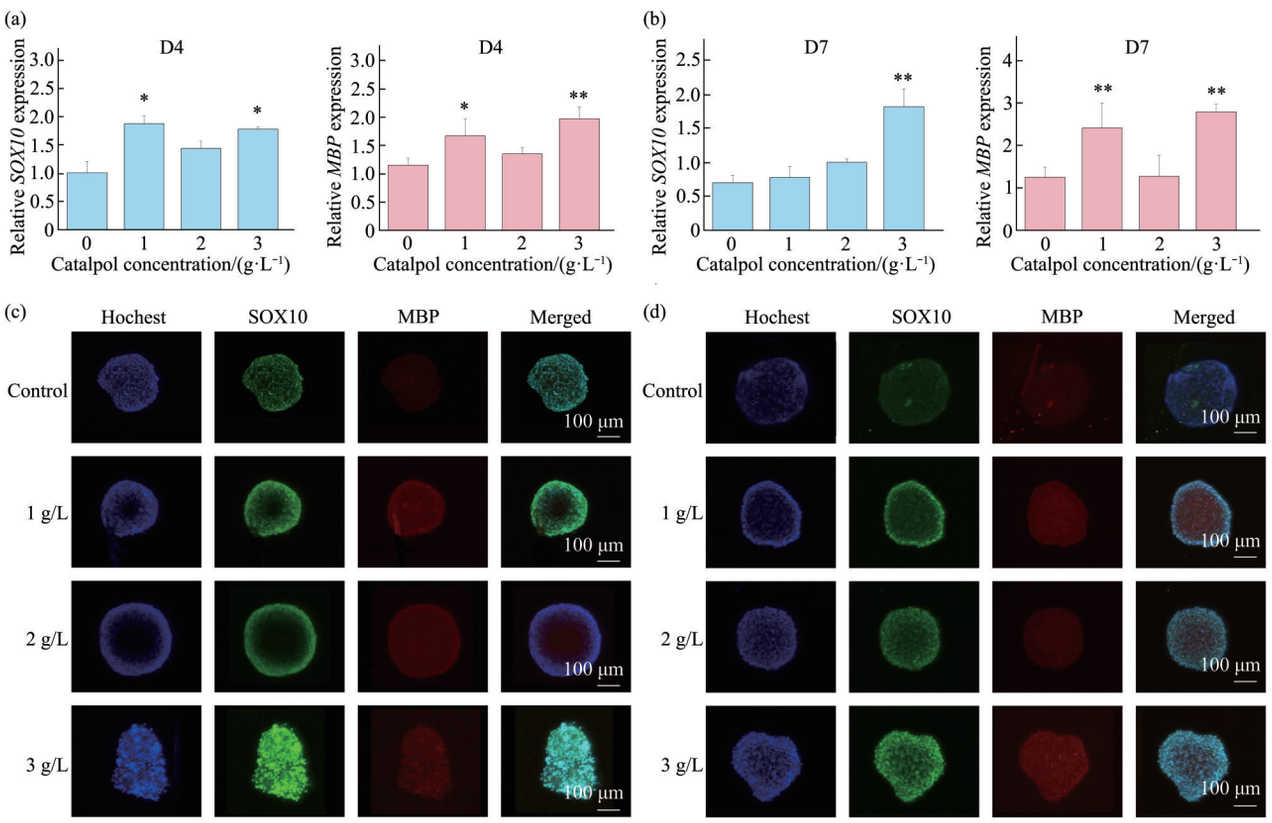

Fig. 3　NSCs differentiation from different concentrations of catalpol

(a, b) qRT-PCR analysis of oligodendrocyte-specific gene expression. mRNA levels of *MBP* and *SOX10* were assessed after 4-day (a) and 7-day (b) perfusion culture with the indicated concentrations of Catalpol (0, 1, 2, 3 g/L). Values are expressed as mean±SD (n=3) relative to the control group (0 g/L). *P<0.05, **P<0.01. (c, d) Immunofluorescence images. Cells were stained for SOX10 (green) and MBP (red) after 4 d (c) and 7 d (d) culture. Nuclei are labeled with Hoechst 33258 (blue).

2.4　The influence of catalpol on Cav−1 expression

To elucidate the role of Cav-1 in the differentiation process of NSCs, we analyzed its expression changes using qRT-PCR. The quantitative qRT-PCR results (Figure 4a, b) demonstrated that catalpol treatment significantly suppressed Cav-1 expression. After 4 d of perfusion culture, the *Cav-1* gene expression levels in the 1, 2, and 3 g/L catalpol groups were downregulated by 68.9%, 16.0%, and 45.4%, respectively, compared to the control group, with the decreases in the 1 and 3 g/L groups being statistically significant (P<0.05). This inhibitory effect became more pronounced and exhibited concentration dependence by day 7 of culture, with expression levels in the concentration groups reduced by 63.5%, 54.2%, and 68.6%, respectively, compared to the control, and all differences reaching a highly significant level (P<0.01). As shown in the immunofluorescence images in Figure 4c, d, co-localization analysis was performed for the Cav-1 (red). This provides a qualitative assessment for the qRT-PCR findings.

2.5　Catalpol promotes oligodendrocyte differentiation by inhibiting the Cav−1 pathway

To measure whether catalpol could accelerate oligodendrocyte differentiation by inhibiting the Cav-1 signaling pathway, we applied methyl β-cyclodextrin (MCD), a specific inhibitor of Cav-1[13]. We used qRT-PCR and immunofluorescence to detect changes in MBP and SOX10 expression following MCD inhibition of Cav-1. After 4 and 7 d of induction, the mRNA expression of *SOX10* was

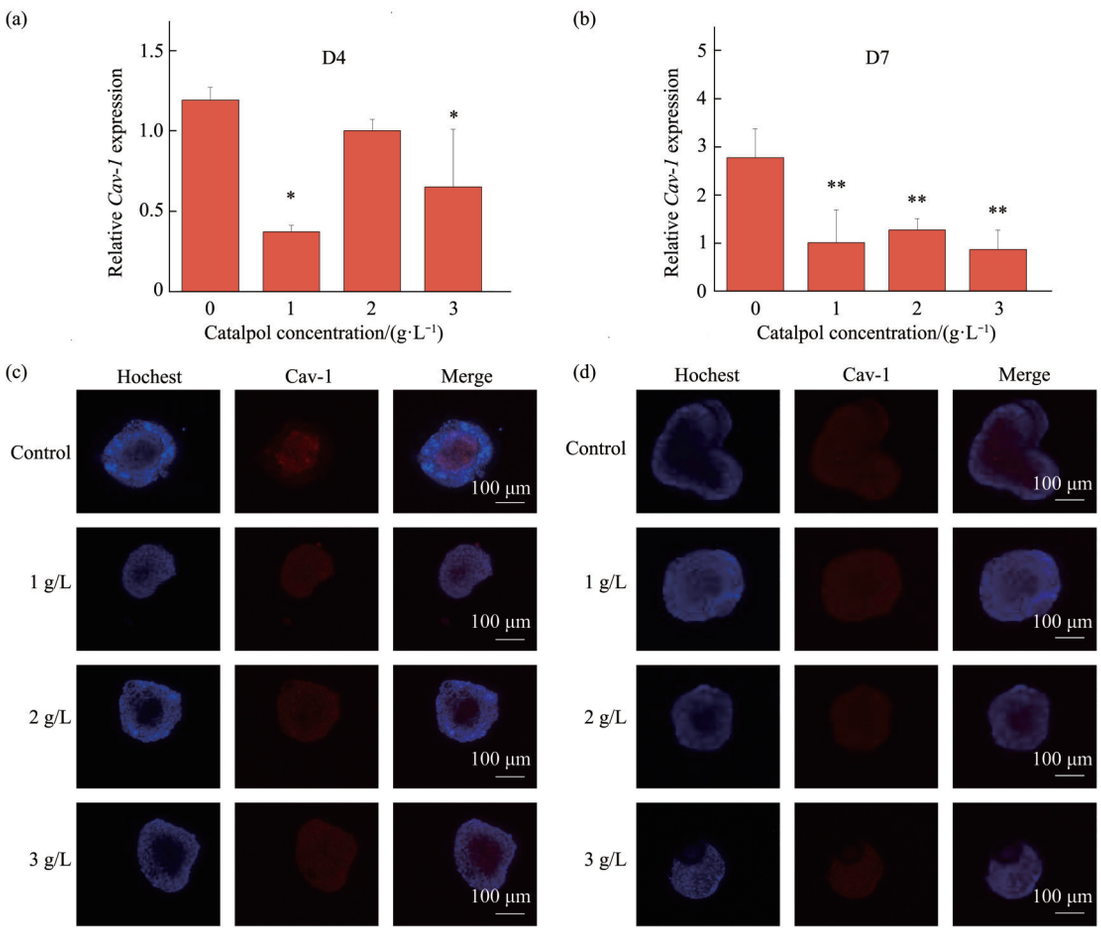

Fig. 4　Cav−1 expression in different concentrations of catalpol after 4 or 7 d of induction

(a, b) qRT-PCR was employed to assess *Cav-1* gene expression at the mRNA level after 4 d (a) and 7 d (b) perfusion culture with the indicated concentrations of Catalpol (0, 1, 2, and 3 g/L). Values are expressed as mean±SD (n=3) relative to the control group (0 g/L). *P<0.05, **P<0.01. (c, d) Immunofluorescence images of Cav-1 expression. Cells were stained for Cav-1 (red) after 4 d (c) and 7 d (d) culture. Nuclei are labeled with Hoechst 33258 (blue).

more strongly increased in the catalpol MCD group than in the catalpol group (P<0.01, P<0.001), and the mRNA expression of *SOX10* was strongly increased in control MCD group compared to in the control group (Figure 5a) after 4 d of induction. After 7 d of induction, the mRNA expression of *MBP* was strongly increased in the catalpol MCD group compared to the catalpol group (P<0.05), and the mRNA expression of *MBP* was strongly increased in control MCD group as compared to that in the control group (Figure 5b) after 4 and 7 d of induction. As shown in the immunofluorescence images (Figure 5c, d), the expression of the oligodendrocyte markers SOX10 (green) and MBP (red) was increased in the catalpol MCD and control MCD groups during the differentiation process, and co-localization analysis of these two markers was also performed. It should be noted that immunofluorescence was only used for qualitative assessment to support the qRT-PCR findings. Collectively, these qualitative results indicated that Cav-1 is involved in the differentiation of NSCs into OLs, and catalpol accelerates the differentiation of NSCs into OLs by inhibiting the Cav-1 pathway.

3　Discussion

PMWI is associated with the subsequent development of cerebral palsy[14]. OLs are an important component of brain white matter, being the source of nerve growth factor and trophic factor in the central nervous system. The central objective of Neurorestoratology is to fundamentally reverse

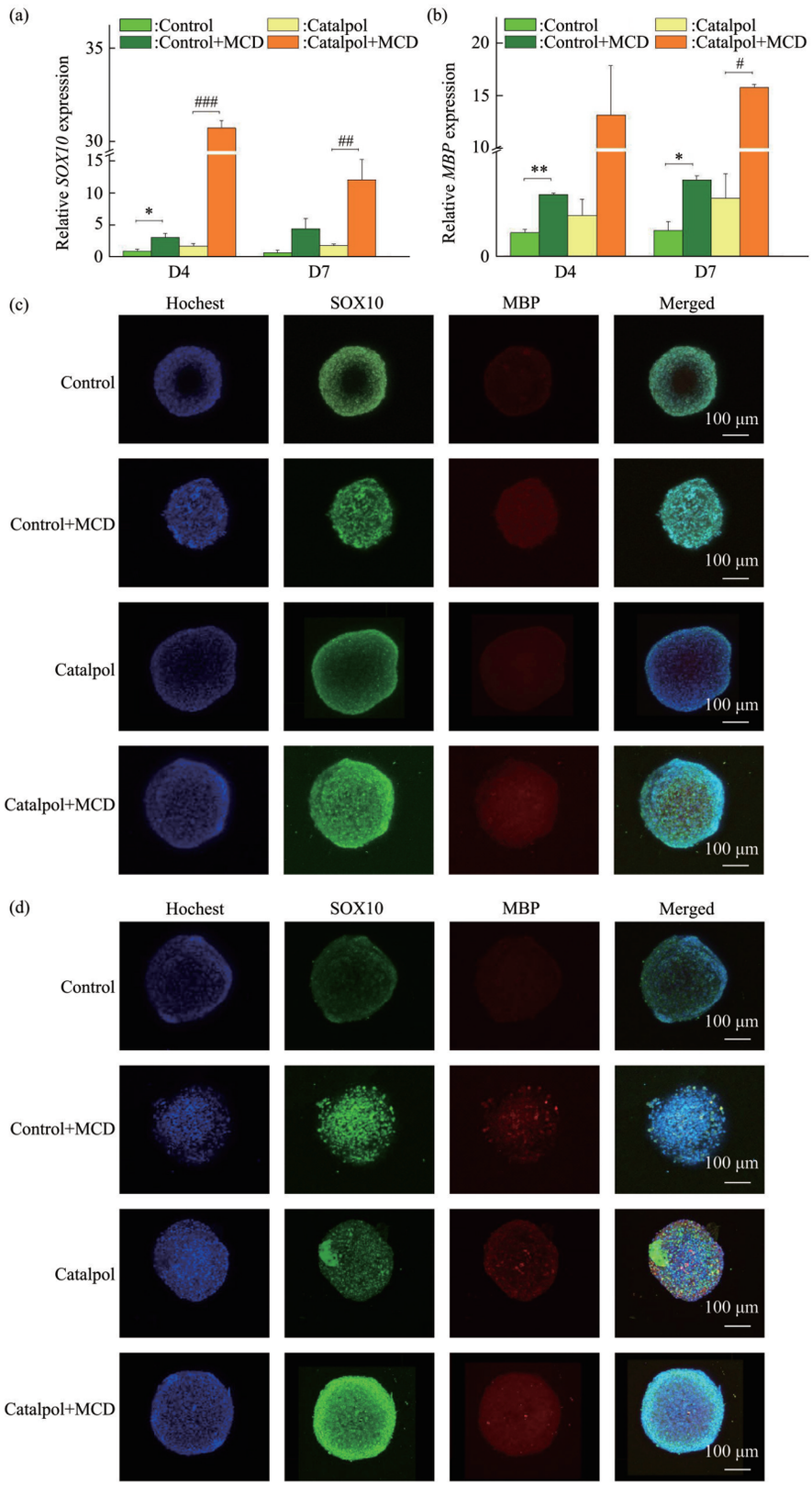

Fig. 5　Comparison of NSCs differentiation into OLs after inhibition of Cav−1

(a, b) qRT-PCR analysis of oligodendrocyte-specific gene expression. mRNA levels of *MBP* and *SOX10* were assessed after 4 d (a) and 7 d (b) perfusion culture under the indicated conditions. Data are presented as mean±SD (n=3). Statistical significance was analyzed between control *vs*. control MCD groups (**P*<0.05, ***P*<0.01) and catalpol *vs*. catalpol MCD groups (#*P*<0.05, ##*P*<0.01, ###*P*<0.001). (c, d) Immunofluorescence images of oligodendrocyte differentiation. Neural stem cells (NSCs) were stained for the transcription factor SOX10 (green) and the myelin marker MBP (red) after 4 d (c) and 7 d (d) culture. Nuclei were counterstained with Hoechst 33258 (blue).

functional impairments by reconstructing damaged neural structures and restoring intercellular communication[15]. Therefore, a treatment method capable of repairing these nerves, when injured, is urgently needed. With advancements in material science and tissue engineering, they have been increasingly adopted for the treatment of degenerative diseases and nervous system injuries[16-17]. NSCs differentiation is affected by many factors, and methods for influencing their transformation into specific nerve cell types remain the focus of research in the field of nerve regeneration[18].

Our study aimed to investigate the role of catalpol, a potential therapeutic for neurodegeneration, in neural differentiation by studying the differentiation of NSCs into neurogliocytes. In this study, we established a 3D culture model of NSCs on a micro-fluidic chip and used it to evaluate the effect of catalpol on NSCs. Cells form 3D tissues inside the human body, but drug testing is often performed using 2D cell cultures. Results obtained using these cultures, which do not represent the actual environment in the body, may fail to accurately predict the body's response to the tested drugs[19]. Liu and others[20] employed an NSCs cell differentiation model to detect neurotransmitters, finding that a 3D culture was better able to protect the drug injury model after neuronal cell differentiation than a 2D culture. Therefore, we expect that the use of 3D culture methods to generate spheroids will become increasingly important for *in vitro* drug screening during drug development[21-22]. In our study, NSCs are cultured as 3D pellets, allowing for the generation of results more reflective of the *in vivo* microenvironment.

Compared to conventional 2D static culture methods, microfluidic chips provide a superior screening and testing platform, as they are better able to simulate the *in vivo* microenvironment[23]. Consequently, employing microfluidic technology to detect drug-related toxicity during the preclinical period of drug evaluation can more accurately indicate the actual clinical efficacy of the drug[24-25]. Microfluidic gradient chips have several advantages, including high throughput and simple operation. In addition, they can also economize experimental time, generate stable drug concentrations, enable real-time observation of the action of drugs on cells, and allow continuous perfusion cultures to be stably maintained for extended periods[26-27]. The CGG chip designed in this study can generate a stable gradient and connect to 12 culture chambers for parallel testing at multiple concentrations. However, we also recognize that, compared to the recently reported "organ-on-a-chip" or "intelligent-responsive" microfluidic platforms, the cell models and drug administration modes employed in this study remain relatively fundamental. Furthermore, the current gradient generation module can only provide linear concentration ramps and is limited to endpoint detection, making it difficult to simulate the *in vivo* pharmacokinetic fluctuations characterized by "peak-valley-baseline" profiles. To enhance physiological relevance, future work will focus on incorporating vascular endothelial cells and microglia into the chip to construct a "neuro-vascular-immune" unit, enabling a more comprehensive evaluation of catalpol's efficacy and mechanisms[28]. Inspired by Vollertsen *et al.*' s "fluid circuit board" pulsed valve array[29] and Wang *et al.*' s multi-endpoint real-time monitoring strategy in organoid-on-a-chip systems[30], the next step will involve upgrading the CGG to a programmable "pulse-decay" gradient unit. This advancement will allow synchronous monitoring of NSCs viability, differentiation, and temporal changes in inflammatory factors within the same chip, thereby providing deeper insights into the dose-response relationship and optimal dosing regimen of catalpol.

Caveolae are a specific cytomembrane structure present on the plasma membranes of many vertebrate cell types. Cav-1 is a marker protein of caveolae, and is closely involved in the function and development of the nervous system. Zhao *et al.*[31] found that Cav-1 can inhibit the differentiation of PC12 cells into neurons, while Li *et al.*[32] found that the differentiation of NSCs into OLs was increased by knocking out the Cav-1 gene in mice. Baker *et al.*[33] also suggested that Cav-1 knockout is conductive to the differentiation of NSCs into OLs. Zhou *et al.*[34] have observed that catalpol can lower Cav-1 titers, improving the spatial memory of diabetic rats. To investigate the role of Cav-1 in the differentiation of NSCs into OLs and the induction mechanism of catalpol, this study detected changes in Cav-1 mRNA expression using qPCR. The results showed that after induction with different concentrations of catalpol for 4 to 7 d, Cav-1 mRNA expression was consistently lower than in the uninduced control group, indicating

that catalpol exerts an inhibitory effect on Cav-1. Although limited by the cell quantity available on the chip, this study could not validate changes in Cav-1 protein levels *via* Western blot. However, existing literature suggests that alterations in Cav-1 mRNA are generally accompanied by consistent changes in its protein expression[35-36]. In the future, further verification is required by expanding the cell culture scale or introducing protein detection technologies with higher sensitivity. To further verify the functional role of Cav-1, we employed the inhibitor MCD for intervention. The results demonstrated that combined treatment with catalpol and MCD significantly enhanced the mRNA expression levels of the oligodendrocyte markers *MBP* and *SOX10*: expression in the catalpol group with MCD was significantly higher than in the group treated with catalpol alone, while in the control group with MCD, expression was also significantly elevated compared to the untreated control group. Collectively, these findings suggest that catalpol may promote the differentiation of NSCs into OLs by reducing Cav-1 mRNA levels, providing important insights for further elucidating the mechanism by which catalpol facilitates differentiation.

In summary, we successfully established a 3D system mimicking the *in vivo* microenvironment and allowing for different drug concentrations to be tested simultaneously *in vitro*. Our findings may facilitate the development of a new model for NSCs differentiation. Understanding NSCs differentiation in reconstituted *in vivo*-like microenvironments could ultimately be of great importance for stem cell research targeting CP, Alzheimer's disease, Parkinson's disease, spinal cord injury, and multiple sclerosis[37-39].

4 Conclusion

In this study, we engineered the first microfluidic platform capable of generating a seamless, on-chip concentration gradient while simultaneously perfusing three-dimensional NSCs spheroids—thereby creating a physiologically relevant milieu to dissect the impact of catalpol on NSCs viability and oligodendrocytic fate. Within the 0−3 g/L window, catalpol exhibited no cytotoxicity yet orchestrated a robust, dose-dependent specification of NSCs toward the OLs lineage. Mechanistically, we uncovered a reciprocal relationship between oligodendrocytic commitment and Cav-1 expression; functional silencing of Cav-1 with β-cyclodextrin phenocopied catalpol's pro-oligodendrogenic effect, confirming that catalpol exerts its instructive influence *via* Cav-1 suppression. Collectively, these findings not only illuminate the catalpol-Cav-1 axis as a pivotal determinant of NSCs fate, but also establish a microenvironment-faithful *in vitro* paradigm for interrogating traditional Chinese medicine monomers in periventricular white-matter injury and cerebral palsy, thereby opening a translational avenue for stem-cell-drug synergy in repairing neonatal white-matter damage.

Acknowledgements We extend our heartfelt thanks to Prof. REN Yan of The First Affiliated Hospital of China Medical University, Prof. ZOU Wei of Liaoning Normal University, Prof. MA Jing-Yun of The First Affiliated Hospital of Dalian Medical University, and Prof. WEI Wen-Juan of The First Affiliated Hospital of Dalian Medical University, for their invaluable guidance and assistance in the preparation of this manuscript.

Supplementary Available online (http://www.pibb.ac.cn, http://www.cnki.net):
PIBB_20250337_Figure_S1.pdf
PIBB_20250337_Figure_S2.pdf

References

[1] Marefi A, Husein N, Dunbar M, *et al*. Risk factors for term-born periventricular white matter injury in children with cerebral palsy: a case-control study. Neurology, 2022, **99**(22): e2485-e2493

[2] Salomon I. Neurobiological insights into cerebral palsy: a review of the mechanisms and therapeutic strategies. Brain Behav, 2024, **14**(10): e70065

[3] Sosunov S A, Niatsetskaya Z V, Stepanova A A, *et al*. Developmental window of vulnerability to white matter injury driven by sublethal intermittent hypoxemia. Pediatr Res, 2022, **91**(6): 1383-1390

[4] Newville J, Jantzie L L, Cunningham L A. Embracing oligodendrocyte diversity in the context of perinatal injury. Neural Regen Res, 2017, **12**(10): 1575-1585

[5] Bang S, Jeong S, Choi N, *et al*. Brain-on-a-chip: a history of development and future perspective. Biomicrofluidics, 2019, **13**(5): 051301

[6] Maoz B M. Brain-on-a-Chip: characterizing the next generation of advanced *in vitro* platforms for modeling the central nervous system. APL Bioeng, 2021, **5**(3): 030902

[7] Rajalekshmi R, Agrawal D K. Synergistic potential of stem cells

and microfluidics in regenerative medicine. Mol Cell Biochem, 2025, **480**(3): 1481-1493

[8] Chao H W, Chao W W, Chao H M. Catalpol protects against retinal ischemia through antioxidation, anti-ischemia, downregulation of β-catenin, VEGF, and angiopoietin-2: *in vitro* and *in vivo* studies. Int J Mol Sci, 2025, **26**(9): 4019

[9] Hassan M M, Fahmy M I, Azzam H N, *et al*. Multifaceted therapeutic potentials of catalpol, an iridoid glycoside: an updated comprehensive review. Inflammopharmacology, 2025. DOI: 10.1007/s10787-025-01694-1

[10] Cai Q, Yao Z, Li H. Catalpol promotes oligodendrocyte survival and oligodendrocyte progenitor differentiation *via* the Akt signaling pathway in rats with chronic cerebral hypoperfusion. Brain Res. 2014, **1560**: 27-35

[11] Jeon N L, Dertinger S K W, Chiu D T, *et al*. Generation of solution and surface gradients using microfluidic systems. Langmuir, 2000, **16**(22): 8311-8316

[12] Hsieh J, Aimone J B, Kaspar B K, *et al*. IGF-I instructs multipotent adult neural progenitor cells to become oligodendrocytes. J Cell Biol, 2004, **164**(1): 111-122

[13] Kim Y S, Kim J Y, Cho R, *et al*. Adipose stem cell-derived nanovesicles inhibit emphysema primarily *via* an FGF2-dependent pathway. Exp Mol Med, 2017, **49**(1): e284

[14] Vannucci R C, Vannucci S J. Perinatal hypoxic-ischemic brain damage: evolution of an animal model. Dev Neurosci, 2005, **27**(2/3/4): 81-86

[15] Huang H, Sharma H S, Chen L, *et al*. Two sides of one coin: neurorestoratology and neurorehabilitation. J Neurorestoratol, 2024, **12**(2): 100121

[16] Chen J F, Wang F, Huang N X, *et al*. Oligodendrocytes and myelin: active players in neurodegenerative brains?. Dev Neurobiol, 2022, **82**(2): 160-174

[17] Pajevic S, Plenz D, Basser P J, *et al*. Oligodendrocyte-mediated myelin plasticity and its role in neural synchronization. Elife, 2023, **12**: e81982

[18] Li C, Luo Y, Li S. The roles of neural stem cells in myelin regeneration and repair therapy after spinal cord injury. Stem Cell Res Ther, 2024, **15**(1): 204

[19] David L, Dulong V, Le Cerf D, *et al*. Hyaluronan hydrogel: an appropriate three-dimensional model for evaluation of anticancer drug sensitivity. Acta Biomater, 2008, **4**(2): 256-263

[20] 刘庆喜, 吴婷, 孙贺, 等. 三维神经干细胞分化模型在神经药物检测中的应用. 中国细胞生物学学报, 2015, **37**(5): 630-637
Liu Q X, Wu T, Sun H, *et al*. Chin J Cell Biol, 2015, **37**(5): 630-637

[21] Breslin S, O'Driscoll L. Three-dimensional cell culture: the missing link in drug discovery. Drug Discov Today, 2013, **18**(5/6): 240-249

[22] Kwapiszewska K, Michalczuk A, Rybka M, *et al*. A microfluidic-based platform for tumour spheroid culture, monitoring and drug screening. Lab Chip, 2014, **14**(12): 2096-2104

[23] Fu J, Qiu H, Tan C S. Microfluidic liver-on-a-chip for preclinical drug discovery. Pharmaceutics, 2023, **15**(4): 1300

[24] Toh Y C, Lim T C, Tai D, *et al*. A microfluidic 3D hepatocyte chip for drug toxicity testing. Lab Chip, 2009, **9**(14): 2026-2035

[25] Fernandes T G, Diogo M M, Clark D S, *et al*. High-throughput cellular microarray platforms: applications in drug discovery, toxicology and stem cell research. Trends Biotechnol, 2009, **27**(6): 342-349

[26] Wu M H, Huang S B, Lee G B. Microfluidic cell culture systems for drug research. Lab Chip, 2010, **10**(8): 939-956

[27] Wen Y, Yang S T. The future of microfluidic assays in drug development. Expert Opin Drug Discov, 2008, **3**(10): 1237-1253

[28] Wei W J, Wang Y C, Guan X, *et al*. A neurovascular unit-on-a-chip: culture and differentiation of human neural stem cells in a three-dimensional microfluidic environment. Neural Regen Res, 2022, **17**(10): 2260-2266

[29] Vollertsen A R, de Boer D, Dekker S, *et al*. Modular operation of microfluidic chips for highly parallelized cell culture and liquid dosing *via* a fluidic circuit board. Microsyst Nanoeng, 2020, **6**: 107

[30] Wang J, Chen X, Li R, *et al*. Standardization and consensus in the development and application of bone organoids. Theranostics, 2025, **15**(2): 682-706

[31] Zhao Y, Xu P, Hu S, *et al*. Tanshinone II A, a multiple target neuroprotectant, promotes caveolae-dependent neuronal differentiation. Eur J Pharmacol, 2015, **765**: 437-446

[32] Li Y, Lau W M, So K F, *et al*. Caveolin-1 inhibits oligodendroglial differentiation of neural stem/progenitor cells through modulating β-catenin expression. Neurochem Int, 2011, **59**(2): 114-121

[33] Baker N, Zhang G, You Y, *et al*. Caveolin-1 regulates proliferation and osteogenic differentiation of human mesenchymal stem cells. J Cell Biochem, 2012, **113**(12): 3773-3787

[34] Zhou H, Liu J, Ren L, *et al*. Relationship between [corrected] spatial memory in diabetic rats and protein kinase Cγ, caveolin-1 in the hippocampus and neuroprotective effect of catalpol. Chin Med J, 2014, **127**(5): 916-923

[35] Zhang T, Shang F, Ma Y, *et al*. Caveolin-1 promotes the imbalance of Th17/treg in chronic obstructive pulmonary disease by regulating Hsp70 expression. Int J Chron Obstruct Pulmon Dis, 2023, **18**: 565-574

[36] Xu S, Xue X, You K, *et al*. Caveolin-1 regulates the expression of tight junction proteins during hyperoxia-induced pulmonary epithelial barrier breakdown. Respir Res, 2016, **17**(1): 50

[37] Xiao J, Yang R, Biswas S, *et al*. Neural stem cell-based regenerative approaches for the treatment of multiple sclerosis. Mol Neurobiol, 2018, **55**(4): 3152-3171

[38] Pradhan A U, Uwishema O, Onyeaka H, *et al*. A review of stem cell therapy: an emerging treatment for dementia in Alzheimer's and Parkinson's disease. Brain Behav, 2022, **12**(9): e2740

[39] Hosseini SM, Borys B, Karimi-Abdolrezaee S. Neural stem cell therapies for spinal cord injury repair: an update on recent preclinical and clinical advances. Brain. 2024;**147**(3):766-93

梓醇通过小窝蛋白1依赖途径在3D微流控芯片中促进神经干细胞向少突胶质细胞分化*

王亚辰[1,2]　王　亮[1,2]　沈丽明[1,2]　刘　晶[1,2)**]

([1)] 大连医科大学附属第一医院，干细胞临床研究机构，大连 116000；
[2)] 大连干细胞与精准医学创新研究院，大连 116000）

摘要　目的　脑瘫是一种常见的围产期获得性神经发育障碍，脑室周围白质损伤（PWMI）是其主要病理改变，其特征为少突胶质细胞（OLs）丢失及髓鞘崩解。神经干细胞（NSCs）可作为OLs的再生来源，但传统二维（2D）体外体系缺失三维（3D）生理微环境，微流控芯片技术可在干细胞微环境中实现3D微环境培养与浓度梯度的精准调控。梓醇（catalpol）是一种兼具抗氧化与抗凋亡活性的环烯醚萜苷，其在3D仿生条件下驱动NSCs向OLs分化的潜能及分子机制尚不明确。本研究拟构建微流控3D仿生平台，系统评估梓醇促NSCs-OLs分化的浓度效应，并解析小窝蛋白1（Cav-1）依赖途径。**方法**　自主设计微流控芯片，生成0~3 g/L梓醇稳定浓度梯度，并对NSCs 3D细胞球实施连续灌流培养。钙黄绿素乙酰氧基甲酯/碘化丙啶（Calcein-AM/PI）实时监测细胞活力；实时荧光定量逆转录聚合酶链式反应（qRT-PCR）定量与MBP/SOX10免疫荧光定性OLs分化；联合Cav-1抑制剂甲基-β-环糊精（MCD）解析梓醇促NSCs向OLs分化的分子机制。**结果**　梓醇在0~3 g/L范围内无细胞毒性（活力>96%）；3 g/L梓醇显著上调*MBP*与*SOX10* mRNA表达（$P<0.05$，$P<0.01$）。伴随NSCs向OLs分化，*Cav-1* mRNA表达下调；而Cav-1特异性抑制剂MCD进一步抑制Cav-1后，OLs相关基因表达显著升高（$P<0.05$，$P<0.01$）。**结论**　构建了微流控梯度芯片-NSCs 3D细胞球培养体系，发现3 g/L梓醇可有效抑制Cav-1诱导NSCs分化为OLs，为髓鞘再生研究提供新平台。

关键词　梓醇，神经干细胞，少突胶质细胞，分化，小窝蛋白1，微流控芯片
中图分类号　R318　　**DOI**：10.3724/j.pibb.2025.0337　　**CSTR**：32369.14.pibb.20250337

* 辽宁省“兴辽英才”计划（XLYC1902031），大连市科技创新人才创新支持计划（2022RG18）和辽宁省教育厅基础研究项目（LJKQZ20222395）资助。
** 通讯联系人。
Tel：0411-83635963，E-mail：liujing@dmu.edu.cn
收稿日期：2025-07-17，接受日期：2025-11-03